APPENDIX C: Fuel Response to Loads

This page is intentionally blank

Appendix C

Fuel Response to Loads

C.1 Fuel Response to Mechanical Loads

C.1.1 Fuel Rod Buckling

For cask vertical drop accidents, the fuel rods in the assemblies are analyzed as long slender columns with intermediate supports provided by the assembly's spacer grids. Since the section of the fuel rod between the bottom two spacer grids supports the weight of the entire rod, only this section of the rod is typically analyzed. For this segment the critical buckling load, α_{cr}, is given by Equation C.1 from Reference C.1.

$$\alpha_{cr} = \frac{\pi^2}{\ell^2} \frac{E_c I_c}{\left(W_c + W_f\right)} \qquad \text{©.1)}$$

where α_{cr} = critical inertia load magnitude for rod buckling (g's)
ℓ = axial length of the fuel rod between two neighboring transverse spacer grids;
$E_c I_c$ = flexural rigidity of the cladding tube column;
W_c = total weight of the fuel rod cladding;
W_f = total weight of the fuel pellets in the fuel rod

Under static and quasi-static loading, where load duration is relatively long, unrestrained lateral buckling and cladding failure (rupture) can be considered synonymous. On-the- other-hand, for dynamic impact events, where load duration may be on the order of only a few milliseconds, exceeding the critical buckling load will not, by itself, cause failure of the cladding. Rather it is the combination of load and load duration that determines whether the cladding reaches its failure strain. However, regardless of whether the analysis is static, quasi-static or dynamic, whether the fuel is bonded or unbonded to the cladding, or whether the fuel is in granular or solid form, all (100%) of the fuel weight must be included in the buckling process (Reference C.1).

Table C.1 lists the specifications of fuel rods in BWR 7x7, 8x8 and 10x10 assemblies that could be loaded into the MPC at a BWR site. Table C.1 also lists the specifications of a fuel rod in a PWR 15x15 assembly. Even though a PWR assembly would not be contained in a MPC at site, it was selected to illustrate the methodology for fuel response to drop impact, because PWR fuel rods are generally more vulnerable to impact events than BWR fuel rods (Reference C.5). This can be seen by comparing the static buckling loads of the fuel rods in Table C.1. Therefore, to bound the BWR Assemblies, a PWR 15x15 fuel rod was used to illustrate the methodology.

C.1.2 Methodology and Modeling

The peak g loads imposed on a fuel rod from the vertical drop scenarios considered in the PRA far exceed the elastic buckling load of the fuel rods in the assemblies listed in Table C.1. Therefore, to determine the strain ductility demand on the fuel cladding, the inelastic buckling capacity of the fuel rods must be considered. The approach taken here is to analyze the fuel rod as an elastic plastic beam-column with

initial curvature under dynamic impact. Failure of the fuel rod is determined by comparing the maximum strain in the cladding to a strain limit based on experimental data.

Table C.1: BWR 7x7, 8x8, and 10x10 Fuel Bundle Parameters Used to Calculate Buckling Loads for Vertical Drop Scenarios

Rod Array	BWR 7x7	BWR 8x8	BWR 10x10[1]	PWR 15x15
Fuel Length, in (m)	144 (3.66)	144 (3.66)		154 (3.91)
# Spacers	7	7		8
Fuel Rod Length between spacers, in	19.62 (0.50)	19.62 (0.50)		20.5 (0.52)
Modulus, Psi (Pa)	9.8×10^{6} (6.79×10^{10})	9.8×10^{6} (6.79×10^{10})	9.8×10^{6} (6.79×10^{10})	9.8×10^{6} (6.79×10^{10})
Thickness, in (m)	0.035 (8.89×10^{-4})	0.035 (8.89×10^{-4})		0.0265 (0.0007)
Outer Radius, in (m)	0.285 (0.00724)	0.247 (0.00626)		0.215 (0.005)
Inner Radius, in (m)	0.250 (0.00635)	0.212 (0.00537)		0.189 (0.004)
Cross Sectional Area, in^2 (m^2)	0.059 (3.8×10^{-5})	0.050 (3.25×10^{-5})		
I (Cladding Moment of Inertia), in^4 (m^4)	.00211 ($8.8\times10\text{-}^{10}$)	.00133 (5.53×10^{-10})		0.00068 (2.83×10^{-10})
Cladding Weight, lbf (N)	1.98 (8.82)	1.70 (7.55)		7.011[2] (31.19)
Fuel Weight, lbf (N)	9.60 (42.70)	7.46 (33.18)		
P_{cr} (Critical Buckling Load), lbf (N)	531.09 (2362.42)	333.72 (1484.45)	138.00 (613.86)	
α (Critical Buckling Load), g (g)	46 (46)	36 (36)	24 (24)	22 (22)

[1] Missing information is proprietary.

[2] Total fuel rod weight.

Analysis Approach

Since the impact event entails the interaction of potentially hundreds of rods, their spacer grids, tie plates, fuel spacers, basket, cask, and target under dynamic loading, the necessity for computational efficiency can be achieved by modeling a single fuel rod, as was done in some previous studies (Reference C.5 and C.8). Therefore, an explicit finite element analysis model of a single fuel rod with lateral displacement constraints was used to study the inelastic behavior of a fuel rod under dynamic impact loads. The LS-DYNA model used herein was initially developed by Pacific Northwest National Laboratory (PNNL) and the NRC Staff (Reference C.3) to study the behavior of fuel rods under the hypothetical accident conditions described in 10 CFR 71 and was adapted by the NRC Staff to the target characteristics of the drop scenarios evaluated in the PRA.

The model used in this evaluation is based on the following assumptions:

1. It was assumed that all the individual rods of a fuel assembly displace with the same deformed shape. This suggests that the single rod response is characteristic of all rods and can be studied independently. The center fuel rod in the assembly is considered representative of the typical response of the cross-section of rods through the whole assembly.
2. It was assumed that all bending deformations occurred in a single plane, although an actual assembly could exhibit bending deflections and/or twisting within the fuel compartment. This assumption also allows only half of the fuel rod to be modeled.
3. The 3D finite element model uses a shell element to model the mass and stiffness properties of the cladding cross section, but no comparable representation of the fuel was included. This assumption, which is consistent with standard fuel rod buckling analysis, provides a realistic conservative representation of the fuel by discounting any contribution of the fuel pellets to the fuel rod's flexural rigidity, but, at the same time, including 100% of their mass contribution by lumping fuel mass at each shell node of the cladding. An accurate account of the pellet-to-cladding interactions would be difficult to quantify considering the limited information available. However, to overcome unrealistic ovalization of the open cross-section, nonlinear single degree-of-freedom springs were included to represent a Hertzian-type contact between the cladding and the fuel during lateral deformation.
4. Spent fuel rods will typically exhibit deviations from straightness after exposure to a neutron flux (Reference C.5). For rods mounted within an assembly using spacer grids, the unsupported sections of rod tend to bow out as a result of the assembly's position in the core and the fuel rods location within the assembly (i.e., proximity to a moderator rod, etc. Accordingly, a small amount of rod bowing was introduced to facilitate computation. (See discussion below.)
5. The spacer grids are composed of a small array of leaf springs that hold the rods within the assembly. The spacer grid springs are assumed to provide lateral support to the fuel rods with a prescribed nonlinear force-deflection curve. No rotational support is accounted for, and the grids cannot slide axially relative to the rod.
6. The cask was included in the model to capture the fuel rod and cask dynamics. This was achieved by defining a point mass to represent the cask (equal to the total physical mass of the transfer overpack and MPC divided by the total number of fuel rods accommodated in the cask).
7. The target stiffness is modeled with a cask-to-ground spring defined by a constant force-deflection curve whose magnitude is determined through an iterative process to match the deformation characteristics of the MPC base plate for each drop scenario.

Model Geometry and Details

A drawing representing the single fuel rod model is shown in Figure C.1. It is composed of a single fuel rod, a lumped cask mass, springs representing the spacer grids, contact surfaces representing the basket compartment wall, and a spring representing the target stiffness (cask-to-ground/impact limiter). Several views of the actual finite element mesh are shown in Figure C.2. In this figure, the views shown are a) the entire model, b) top of rod with basket compartment walls and spacer grid spring, c) top of rod with fuel pellet springs, and d) bottom of rod with nodes representing the cask and target (impact limiter).

The typical fuel assembly rod is composed of cylindrical fuel pellets within a tubular cladding material that has reinforced end thimbles and an internal spring to minimize gap between the pellets at all times.

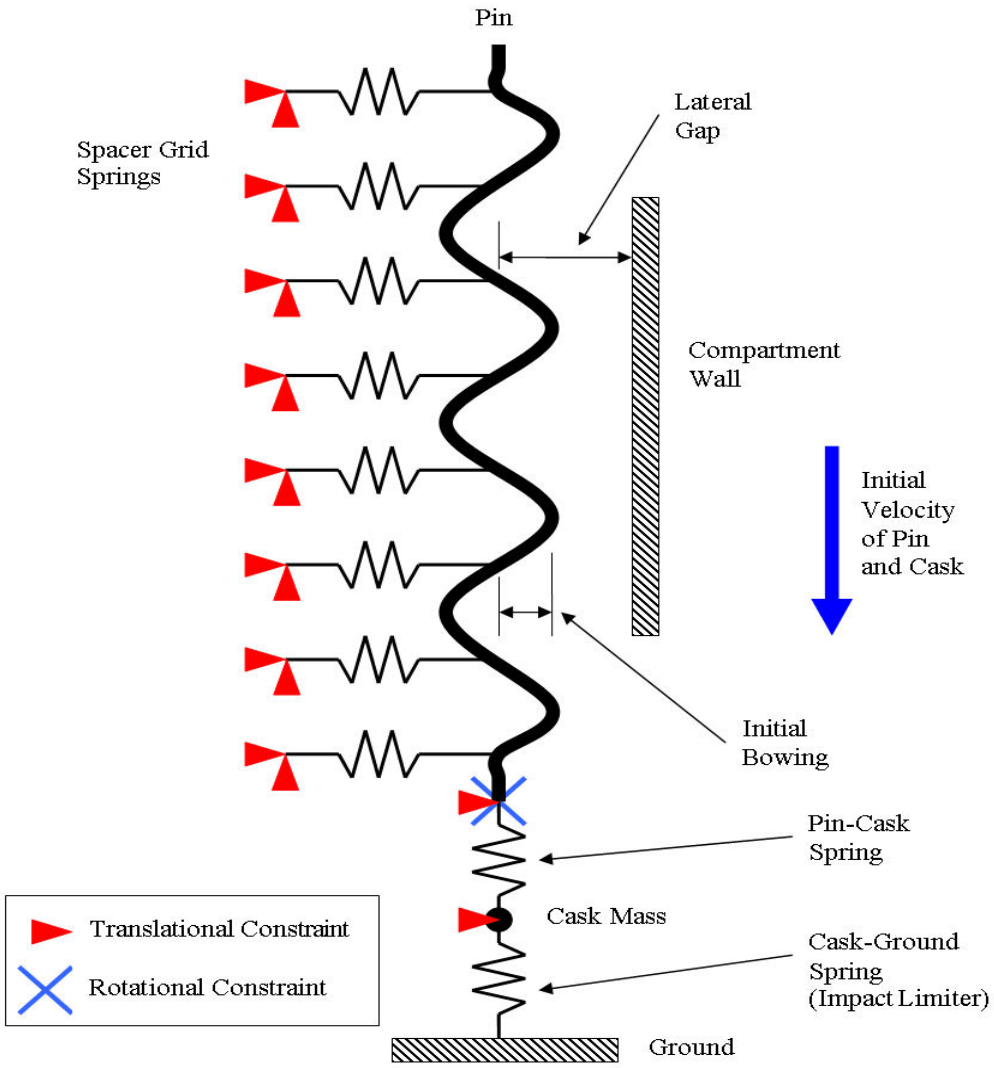

Figure C.1. Single Fuel Rod model.

The rod was modeled using shell elements with appropriate thickness and diameter to represent the cladding, and included about 20,000 elements and 10,000 nodes. The shell element sizing provided sufficient resolution to accurately capture the stress state, as demonstrated through sensitivity studies.

Fuel Rod

The rod was modeled with an initial bow geometry of 0.010" between the spacer grids. The bow between grid spacers was calculated from the overall assembly bow based on the guidance in Reference C.7. It was assumed that the rod had an initial constant curvature in these sections. At the rod ends, it was assumed that they had no initial rotation and that this condition would exist due to the constraint provided by the upper and lower tie plates.

Grid Spacers

The spacer grids are arrayed structures that provide intermediate support to the fuel rods in the assembly. The grids are composed of small leaf springs that ensure proper spacing of the rods in the assembly array.

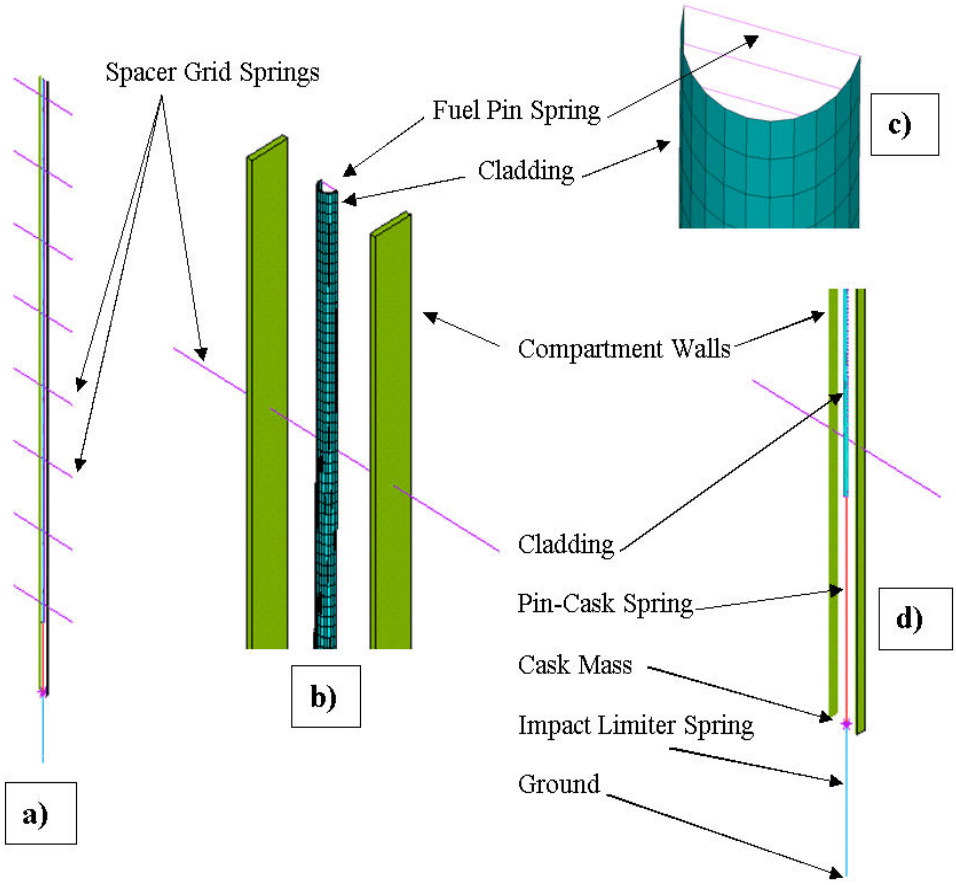

Figure C.2. Single rod model showing a) the entire model, b) top of rod with basket compartment walls and spacer grid spring, c) top of rod with fuel pellet springs, and d) bottom of rod with nodes representing the cask and target (impact limiter).

The grids were assumed to provide lateral support to the rod at eight intermediate locations (Figure C.1) according to the fuel geometry considered. This contribution was represented by sets of compression-only springs attached to each side of the cladding cross-section. These springs behave such that a lateral rod deflection will compress one spring and generate a compressive force, while the spring on other side is unloaded to simulate loss of contact.

Fuel Compartment

Deflection of the fuel rods during an impact event will lead to rod-to-rod and rod-to-compartment wall contact. For an assembly with all rods deforming identically, the outer rods will be the first to contact the compartment walls. Additional deformation causes the next set of rods to seat against these outer rods. This stacking continues until all rods are compressed against the compartment wall. To implement this behavior in a single rod model, the total lateral distance over which a rod could deform must be determined. The gap was determined by considering the rod diameter, number of rods, and compartment width to determine the total free space in which the center rods in an assembly could unilaterally deform, which in the case of the PWR 15x15 assembly was 1.2 inches. The compartment walls were then modeled as rigid planes fixed in space at the proper lateral gap (Figure C.2). Contact elements were implemented to automatically capture contact between the cladding and the compartment walls.

Rod-Cask-Target Interaction

The cask and target stiffness (impact limiter) contribute significantly to rod dynamics. To include the effects of cask mass on system dynamics, the cask was modeled as a point mass. A compression-only spring was then used between the rod bottom and the cask. A second compression-only spring was then used to simulate the target stiffness and ground contact, where the ground was assumed to be rigid. This model construction permitted the system to impact the target surface; however, any rebounding and loss of contact between the rod and the cask or the cask and the ground would be captured.

Material Properties

Cladding

The temperature-dependent mechanical properties for the Zircalloy cladding material were obtained from PNNL data on high burn-up fuels published in Reference C.4. Since fuel rod buckling under vertical impact is expected to initiate at the bottom of the assembly where the fuel is coolest, a uniform temperature of 572˚F (300˚C) was assumed for the rod. It was also assumed that the high burnup fuel had been irradiated to a neutron flux (fluence) of $12x10^{25}$ n/m^2 and would be subjected to a strain rate during buckling of 10/s. The material property estimates corresponding to these conditions are:

Elastic Modulus = $11.0x10^6$ psi
Yield Strength = $92.4x10^3$ psi
Yield Strain = 0.0084 in/in
Tangent Modulus = $14.5x10^4$ psi
Poisson's Ratio = 0.40

Fuel Pellet Spring

To simulate the fuel pellet's ability to limit gross cladding ovalization when the cladding cross section is subjected to high bending curvature, the fuel pellet was modeled as an equivalent spring. The force-deflection curve for this spring was adapted from the solution of an elastic cylinder compressed between two plates under diametrical Hertzian contact as given in Roark (Reference C.9).

Grid Spacer Spring

The force-deflection curves for the spacer grid springs were taken from Reference C.5. The curves represent elastic deformations from a number of coupled events that take place during the lateral movement of fuel rods in an assembly, including 1) compression of the spacer grid leaf spring, 2) compression of the spacer grid frame, 3) buckling of consecutive spacer grid cells, and 4) crushing of the fuel rod cross-section. The spacer grids at the top and bottom of the assembly are attached to the end plates and are consequently stiffer, so they are represented by a different curve.

Cask-Ground Spring

The cask-ground spring represents the behavior of the target impacted by the cask. This is the major source of energy absorption in the system. The target (impact limiter) is characterized by constant force deflection curve, where the force magnitude is determined through an iterative process to approximately match the deformation characteristics of the displacement time-history of the MPC base plate for each drop scenario. Since one foot is the most frequent height from which a cask could be dropped, it is selected to compare the actual MPC base plate displacement time-history to the displacement time-history used in the fuel rod buckling model. For the one foot drop, Figure C.3 shows the displacement

time-history response of five nodes evenly spaced along the top of the base plate from the centerline of the MPC base plate to the MPC shell. For comparison, Figure C.4 shows the displacement time-history of the cask node in the fuel rod buckling model for the one foot drop.

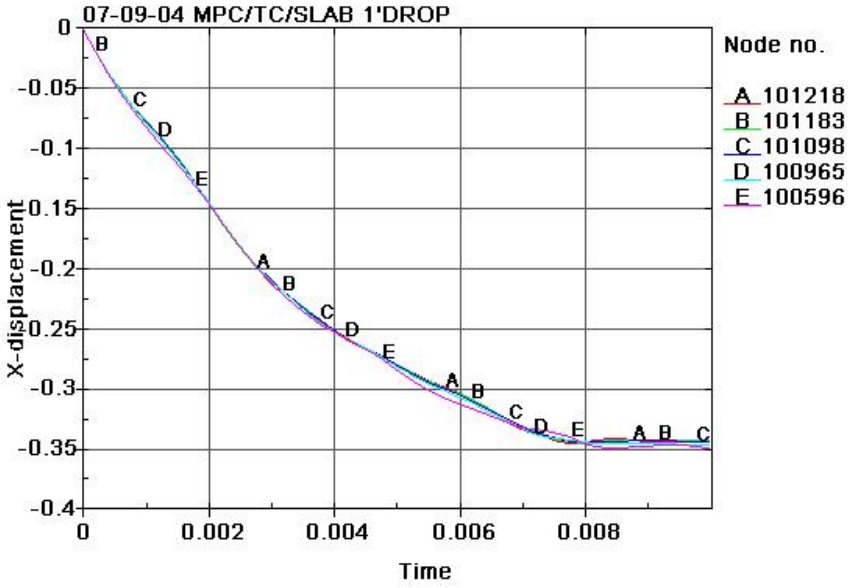

Figure C.3. Displacement of MPC Base Plate Nodes for 1 foot Drop.

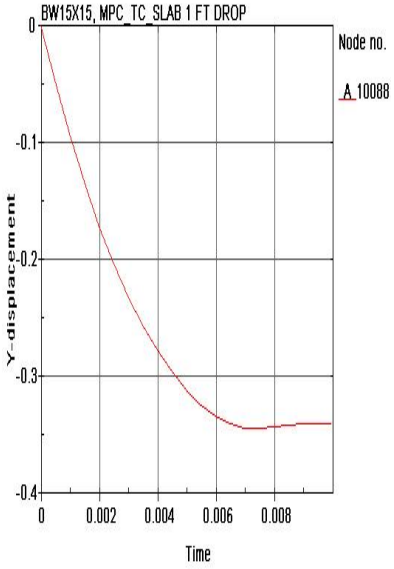

Figure C.4. Displacement of Fuel Rod Model Cask Node for 1 foot Drop.

Boundary and Initial Conditions

The boundary and initial conditions for the model are summarized below:

1. Out-of-plane translations and rotations were constrained along the symmetry plane of the rod.

2. In-plane rotation and lateral translation was constrained at the bottom of the rod. This is based on the assumption that the rods will likely be "jammed" into the bottom tie-plate and restrict rotation and lateral translation.
3. Vertical translation only was enforced for the rod-cask spring, cask, and cask-ground spring.
4. All translations were fixed at the free ends of the spacer grid springs.
5. All translations were fixed at the ground surface.
6. An initial velocity of corresponding to the drop height was applied to the rod and cask nodes.

Fuel Rod Internal Pressure

After a fuel assembly has been exposed to a neutron flux and burned for high burnup durations (>45 GWd/MTU), internal rod pressures due to fission gas generation can range from 1000 to 2200 psi (6.89 to 15.16 MPa). A pressure loading of 1400 psi (9.65 MPa) was applied to the inner cladding surface to simulate the effects of this fission gas generation. This was applied as a preload to the system using a stress initialization procedure prior to solution of the impact event.

C.1.3 Fuel Rod Response and Buckling Behavior

Table C.2 lists the maximum principal strain in the cladding for each drop height evaluated. For the drop of the transfer cask (TC) onto the concrete floor, additional drops of 20 and 55 feet were added to the standard drop heights of 1, 5, 40 70 and 100 feet in order to highlight transitions in buckling behavior or differences in response due to target stiffness.

The results show that the cladding yield strain of 0.0084 in/in is not exceeded until drops of the transfer cask are in the 20 to 40 foot range. The results also show that target stiffness has a significant influence on cladding strain. For example, the 20 foot drop of the TC on to the concrete floor results in a strain less than yield. However the 19 foot drop of the MPC into the storage overpack, which is a much harder impact, produces cladding strains that are ten times greater than yield. This is because the buckling modes resulting from these two impacts are completely different, as will be illustrated later in the discussion.

Figures C.5 and C.6 show the response of the fuel rod for the 20 foot drop at the time when the maximum principal strain in the cladding is reached. Because the material response is entirely elastic and due to the interaction with the grid spacer springs, the maximum response occurs between the 5th and 6th grid spacers during the elastic rebound phase. The maximum lateral displacement of 1.2 inches is equal to the maximum allowable displacement imposed by the basket compartment wall as can be seen in the displacement plot in Figure C.7. It can also be seen from Figure C.6 that no flattening of the rod occurs as it touches the wall.

Figures C.8 and C.9 show the response of the fuel rod for the 40 foot drop at the time when the maximum principal strain in the cladding is reached. As expected, the maximum lateral displacement of 1.2 inches is equal to the maximum allowable displacement imposed by the basket compartment wall, but a slight flattening of the fuel rod against the compartment wall can be seen in Figure C.9.

Table C.2: Maximum Principal Strain in the Cladding for each Drop Height Evaluated.

Event Scenario	Impact Surface (Target)	Drop Height (feet)	Maximum Principal Strain (in/in)
Transfer Cask Vertical Drop	Concrete Floor	1	0.0043
		5	0.0062
		20	0.0072
		40	0.011
		55	0.025
		70	0.037
		100	0.052
MPC Drop into Storage Overpack	Storage Overpack Pedestal	19	0.090

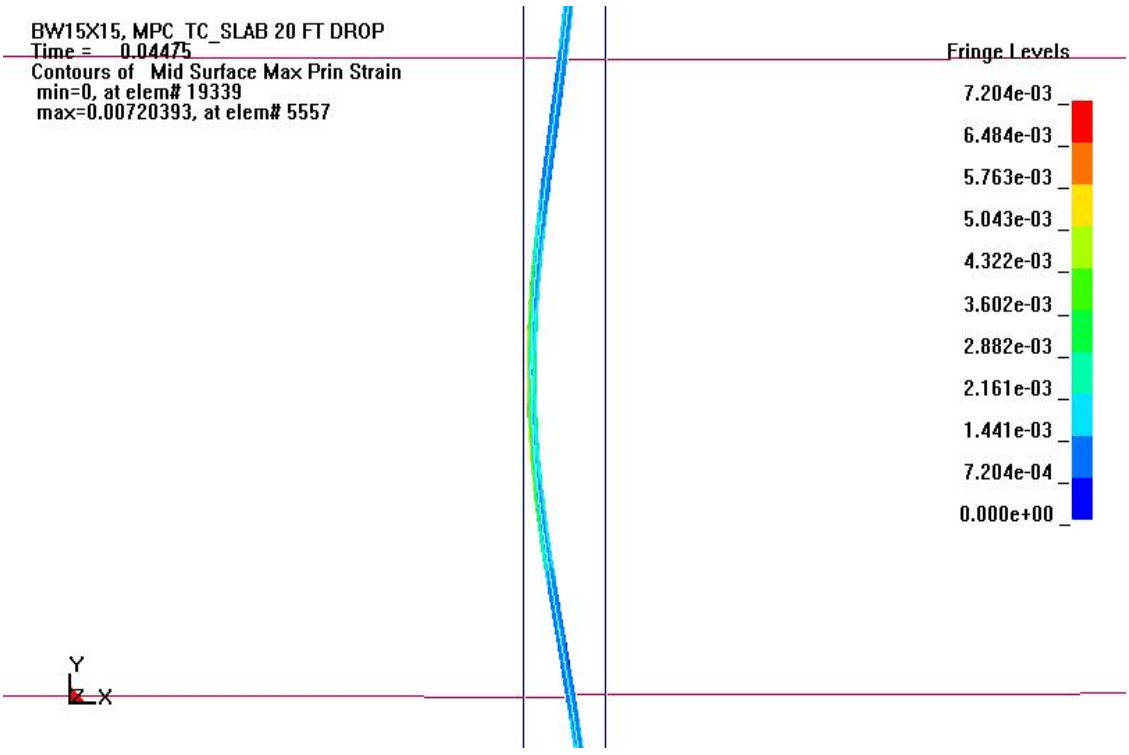

Figure C.5. Maximum Principal Strain at Time of Maximum Response - 20 foot Drop

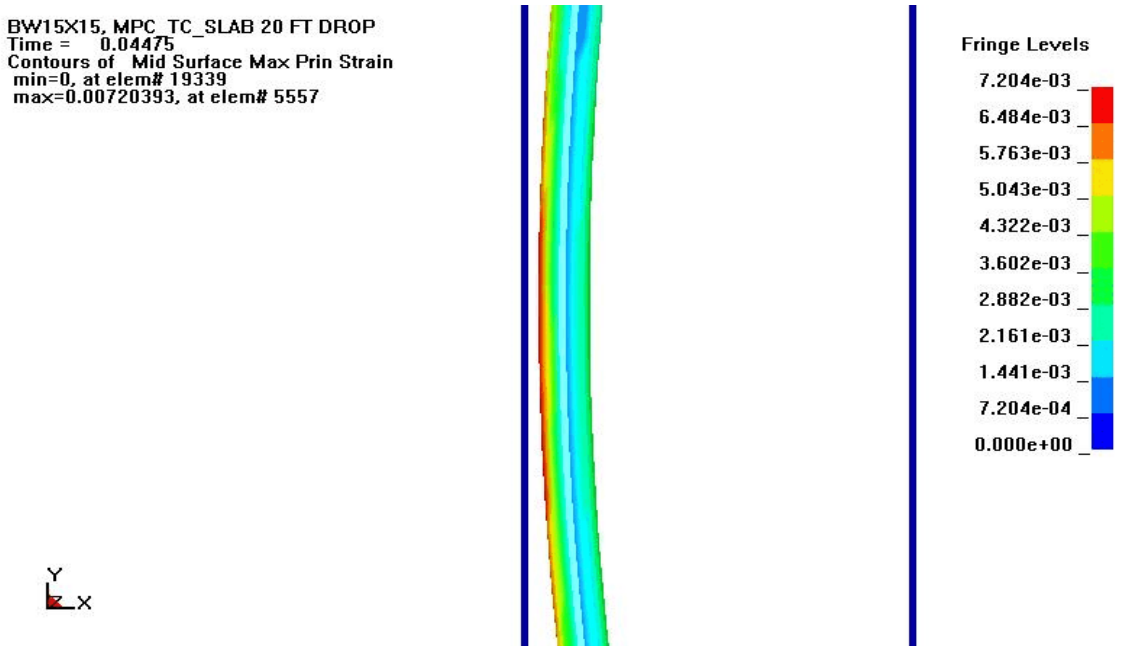

Figure C.6. Maximum Principal Strain at Time of Maximum Response - 20 foot Drop.

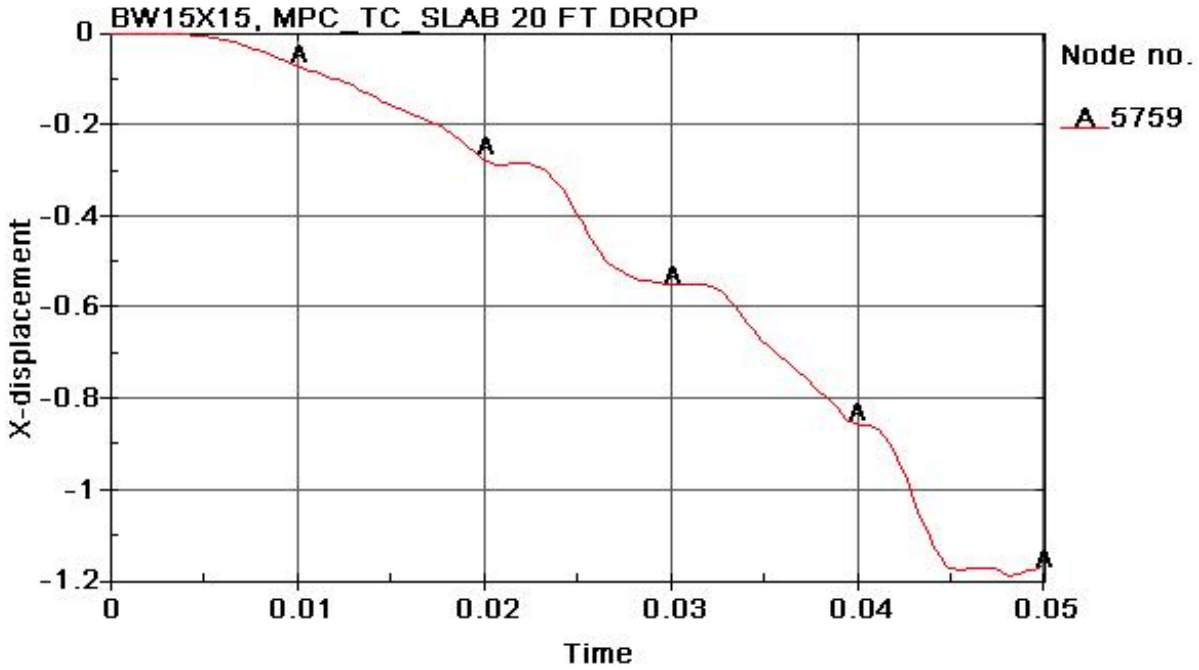

Figure C.7. Fuel Rod Lateral Displacement at point of Maximum Response - 20 foot Drop.

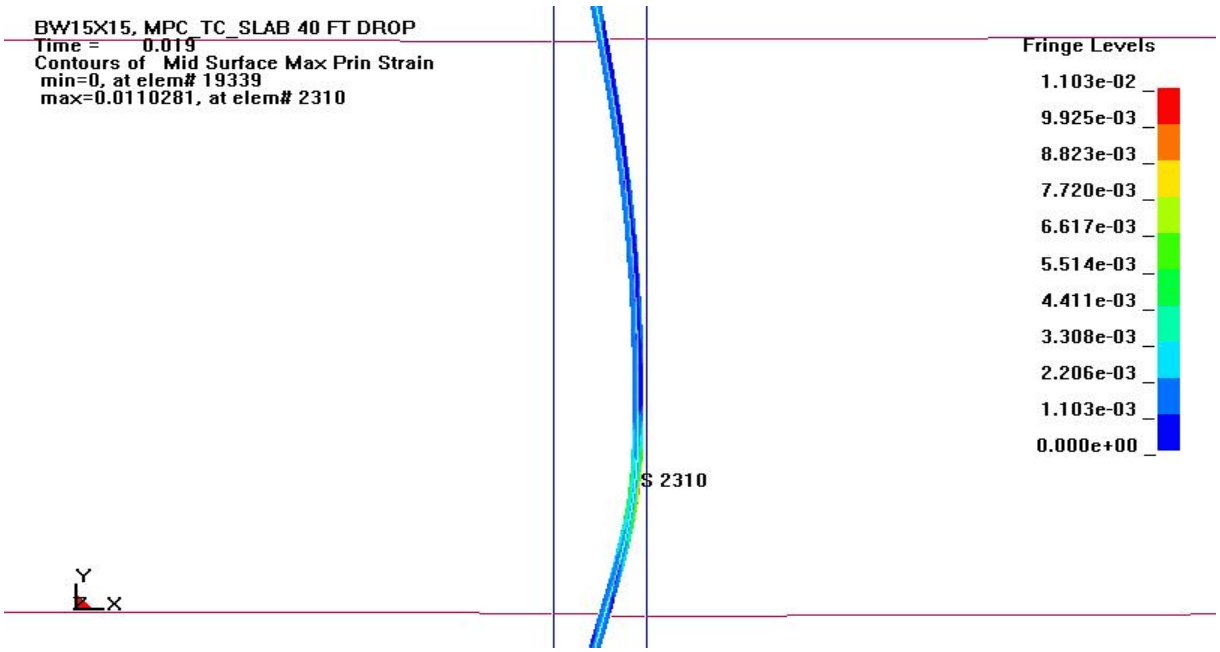

Figure C.8. Maximum principal Strain at Time of Maximum Response - 40 foot Drop.

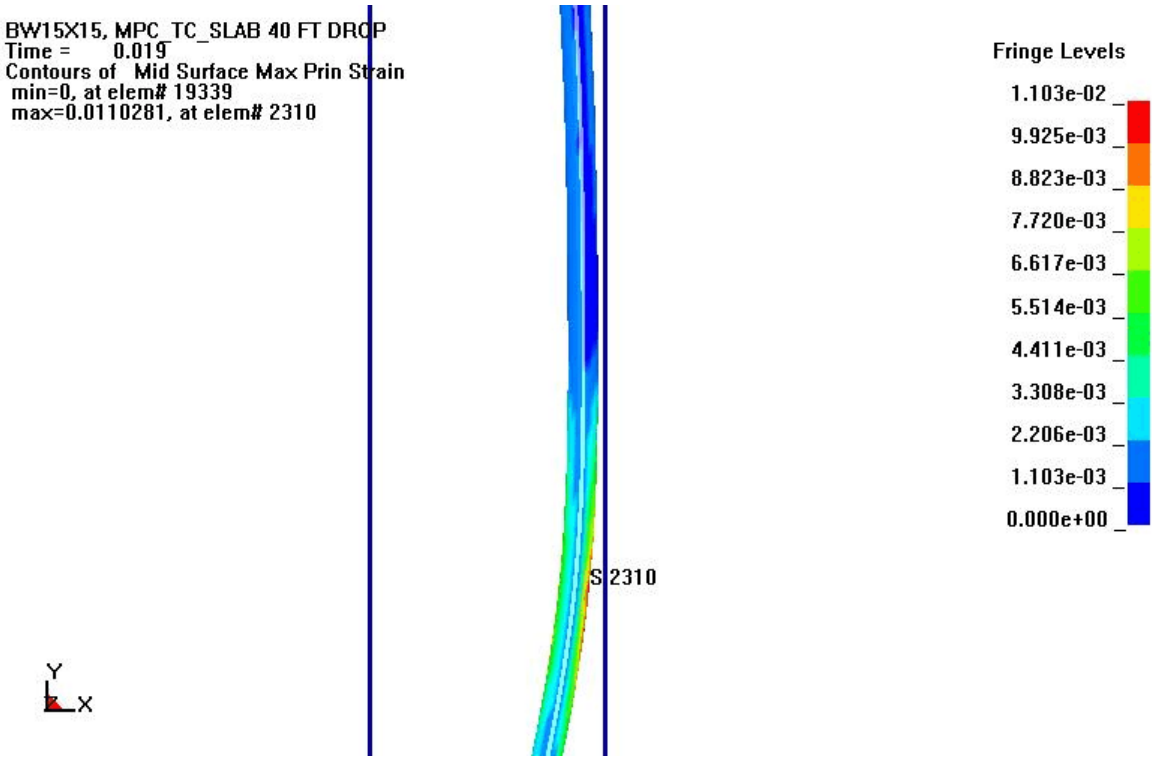

Figure C.9. Maximum Principal Strain at Time of Maximum Response - 40 foot Drop.

Contrast the 40 foot drop response with the response for a 55 foot drop. Figures C.10, C.11 and C.12 show the progression of lateral deformation up to the maximum response at three different times (16.0, 16.5 and 17.0 msec) for the 55 foot drop, and Figure C.13 shows the response over two grid spacers at 17.0 msec. Figure C.14 shows the extreme flattening of the rod against the compartment wall and the concentration of curvature at the location where the rod loses contact with the wall. Figure C.15 is the same as Figure C.14, except that the longitudinal (meridional) strain is shown. The response for the 70 and 100 foot drops are similar.

The response of the fuel rod for the 19 foot drop of the MPC into the storage overpack exhibits completely different behavior than the transfer cask drops onto the concrete floor. Figure C.16 shows the global behavior just prior to the time of maximum response. Figures C.17 and C.18 are close-up views showing the maximum principal strain and the distribution of longitudinal stress at the time of maximum response. The buckled shape is indicative of the classic response of a rod that is unrestrained laterally when impacting a rigid surface (Reference 10). It is clear that the location of the grid spacers does not matter, because the short wavelength mode of buckling is so dominant that it over-rides the flexible lateral resistance of the grid spacers and the lateral bow. As can be seen this free mode of buckling has a much shorter half-wavelength than the distance between grid spacers.

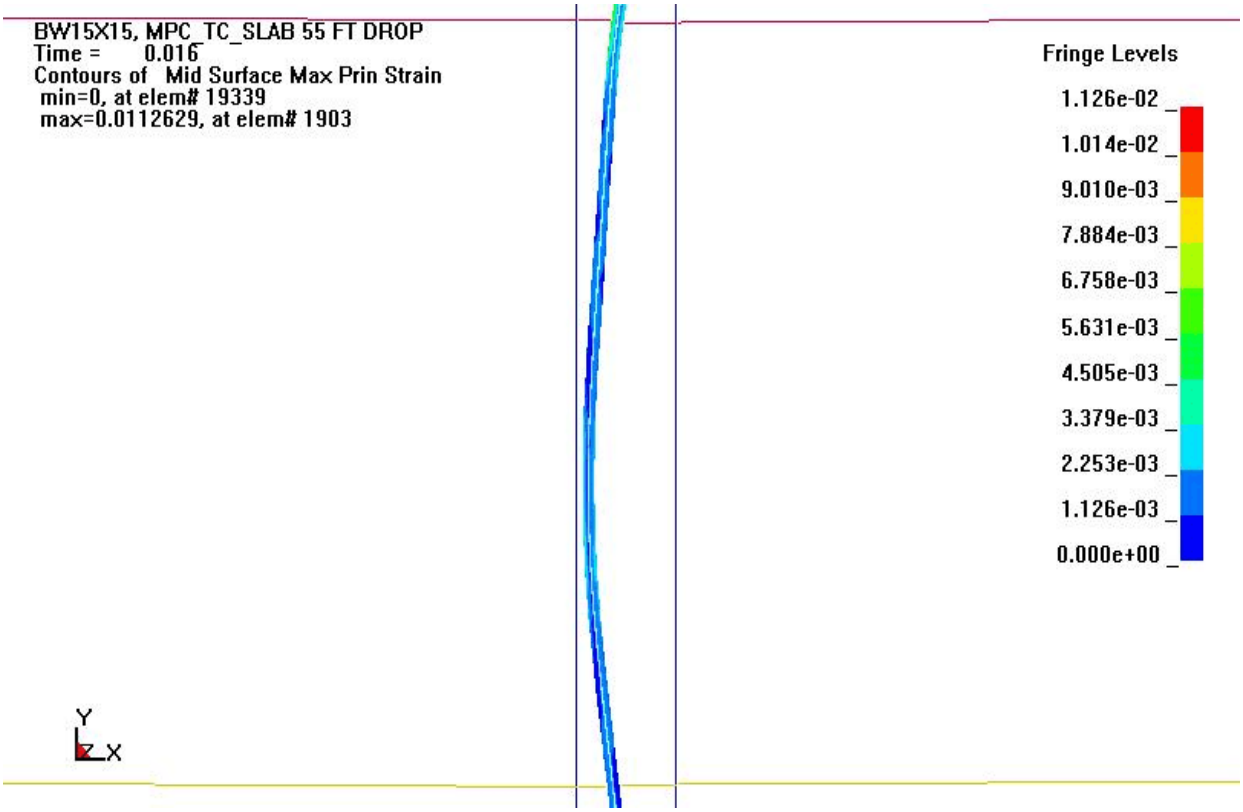

Figure C.10. Maximum Principal Strain at 0.0160 seconds - 55 foot Drop

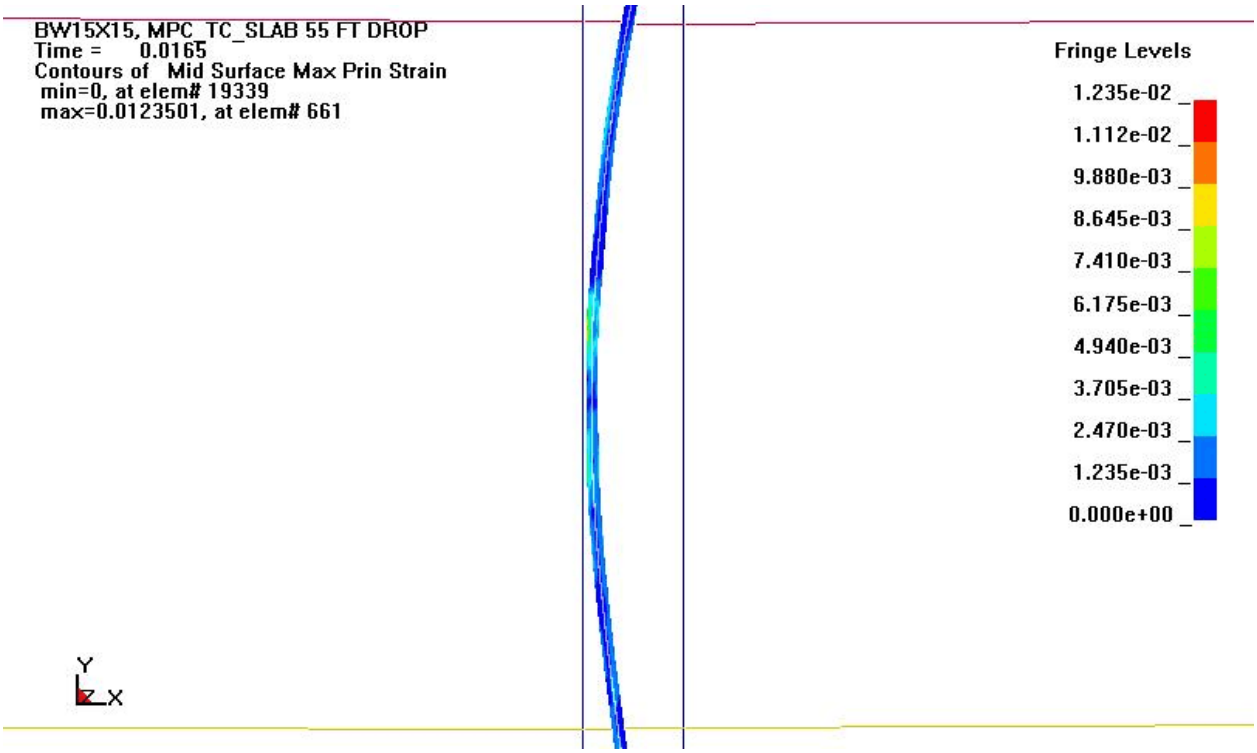

Figure C.11. Maximum Principal Strain at 0.0165 seconds - 55 foot Drop.

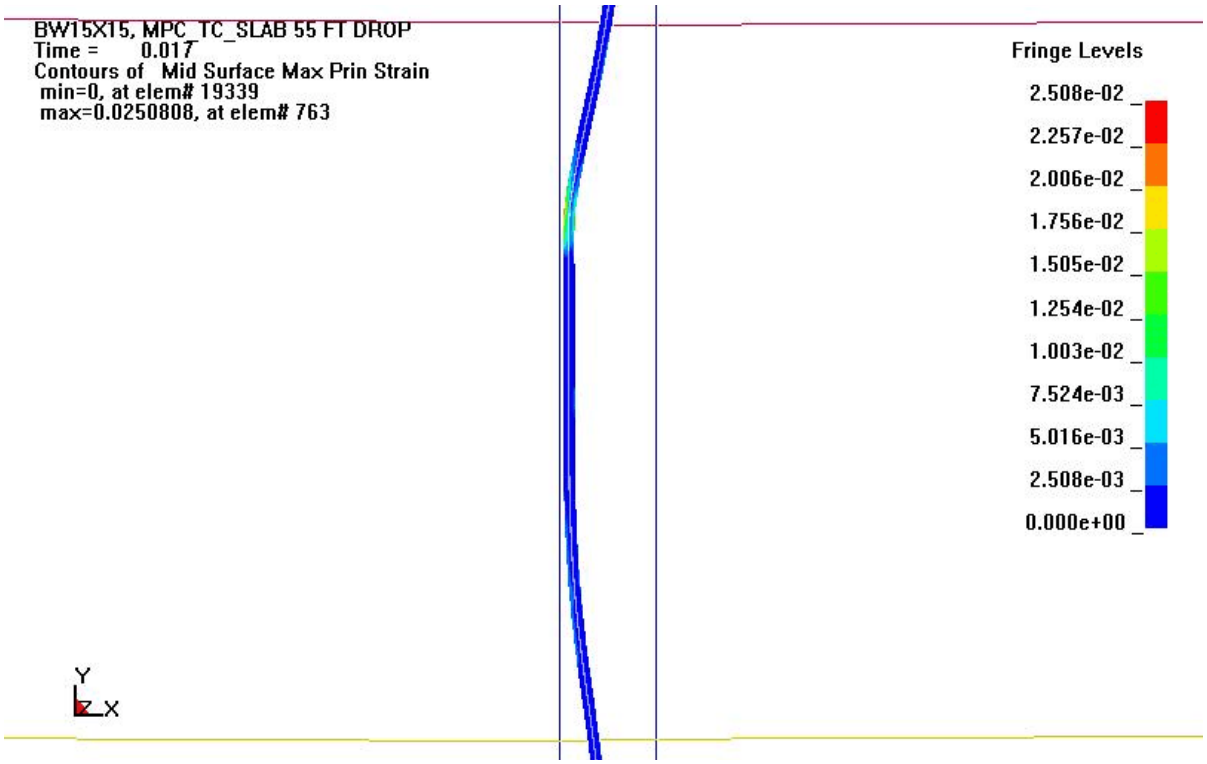

Figure C.12. Maximum Principal Strain at 0.0170 seconds - 55 foot Drop.

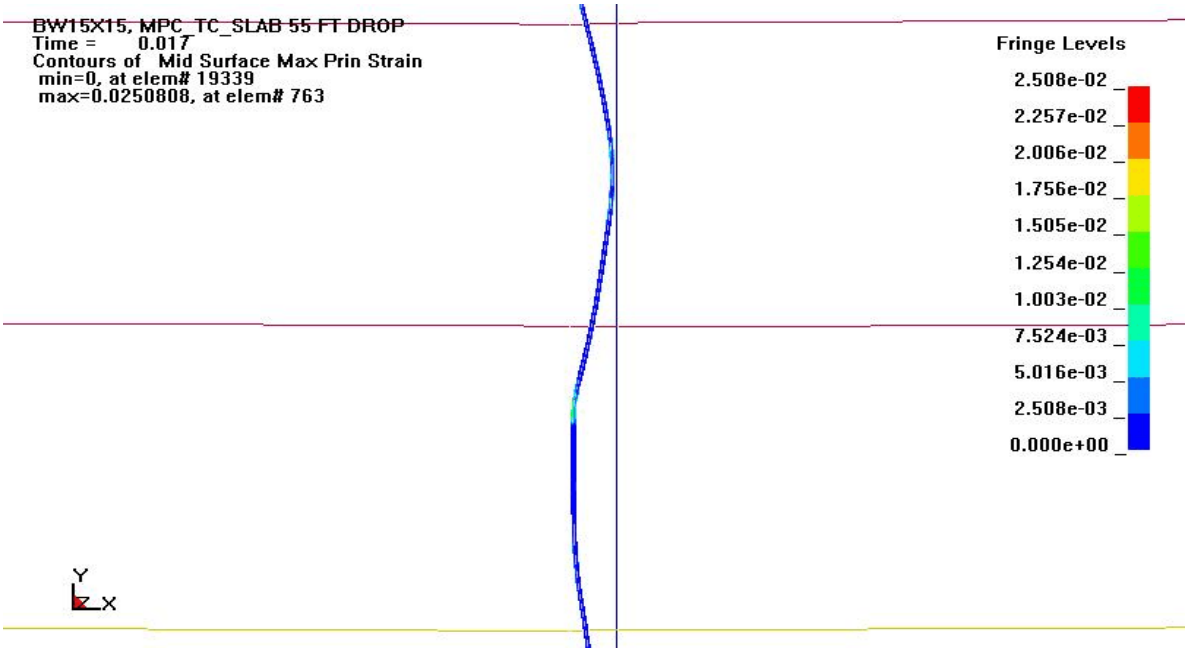

Figure C.13. Maximum Response Shown over the Span of Two Grid Spacers - 55 foot Drop.

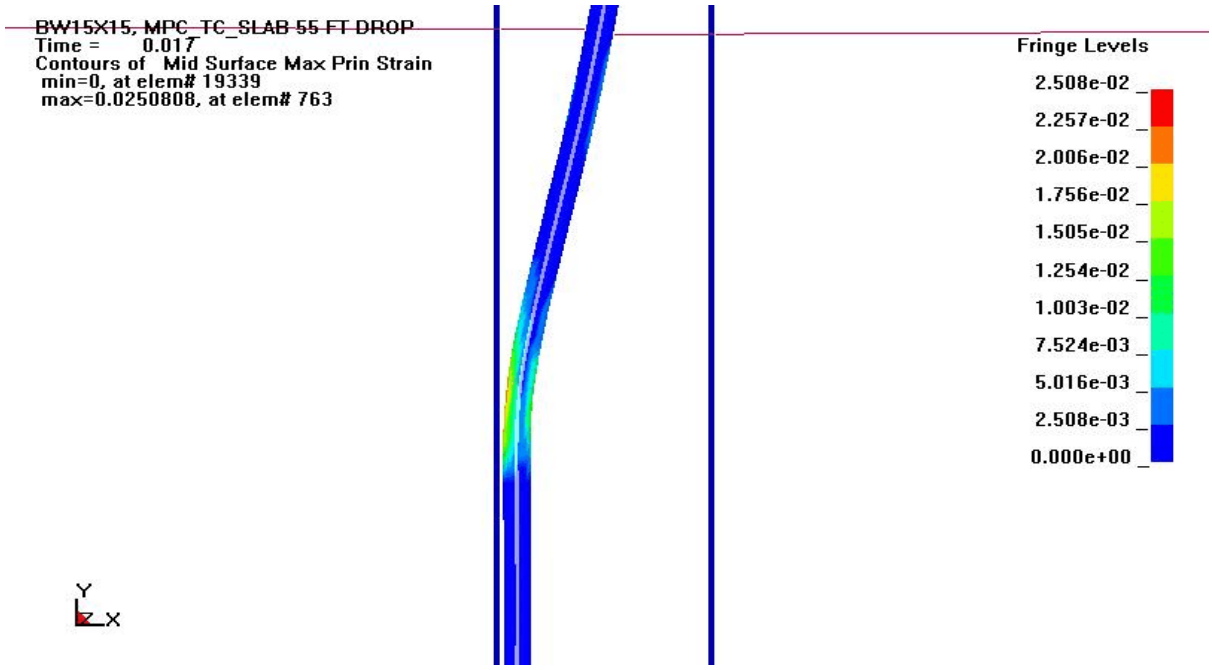

Figure C.14. Shows the extreme flattening of the rod against the compartment wall and the concentration of curvature at the location where the rod loses contact with the wall - 55 foot Drop.

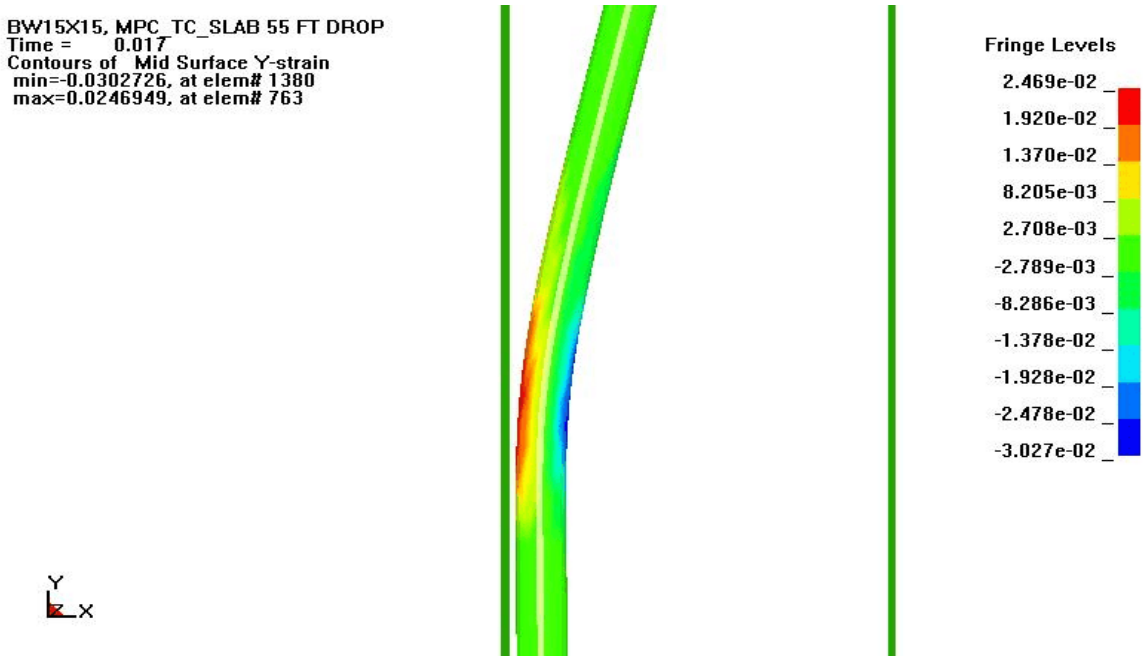

Figure C.15. Closer view of Figure C.14 showing the Longitudinal Strain Distribution - 55 foot Drop.

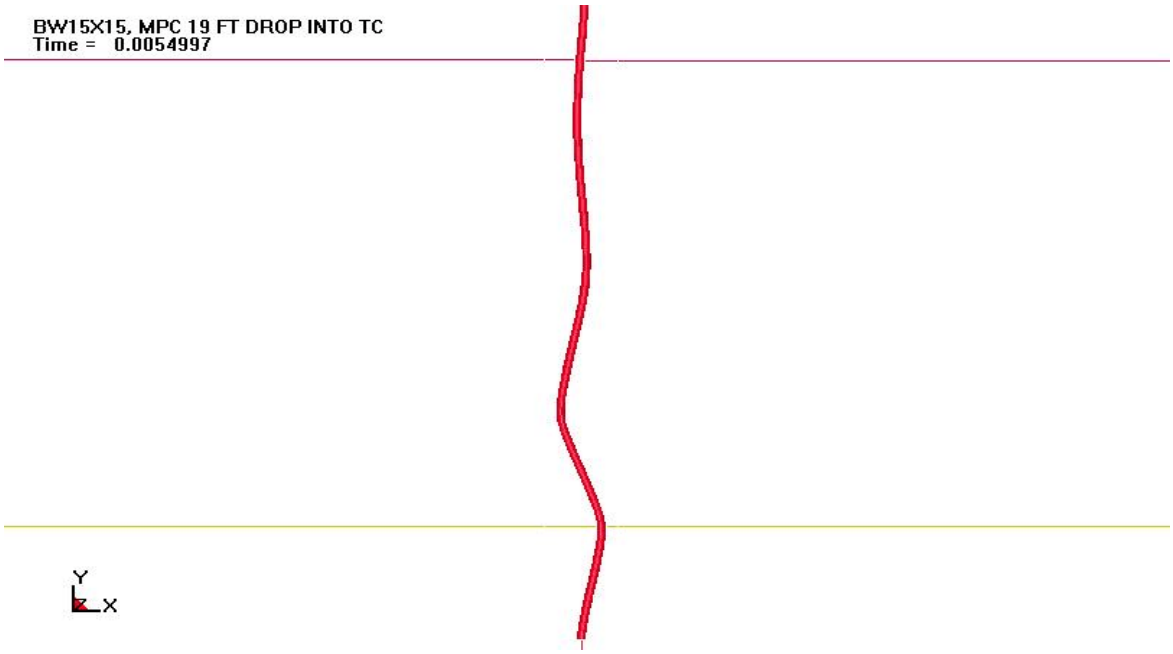

Figure C.16. Buckling Response at the Rod Bottom End just Prior to the Time of Maximum Response - 19 foot Drop of MPC into Storage Overpack.

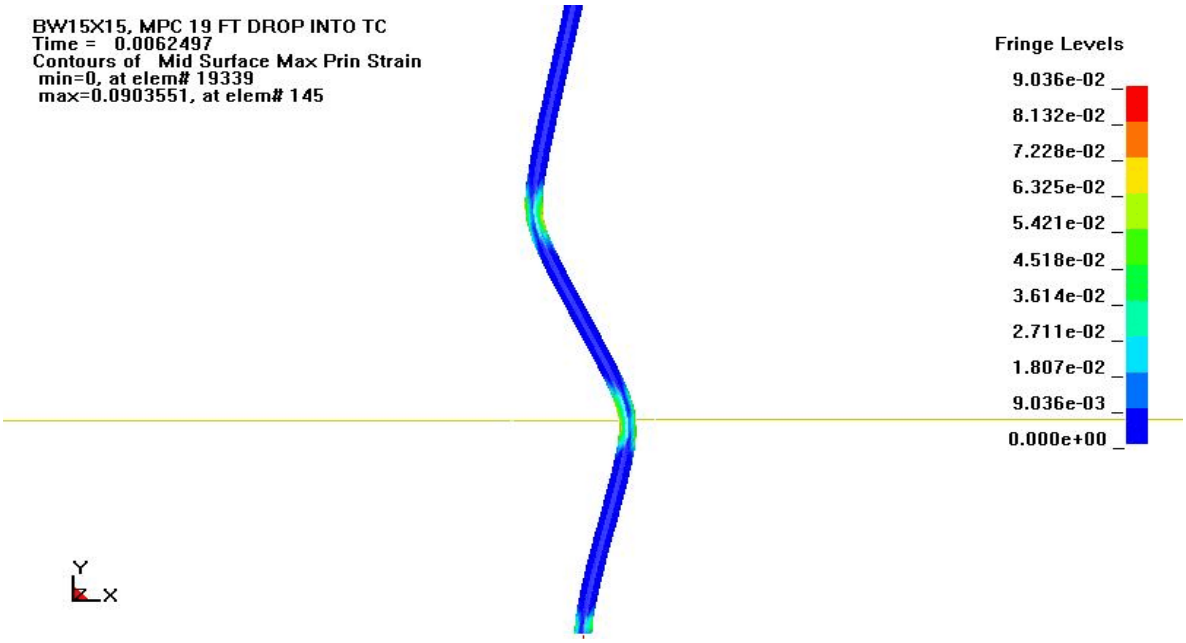

Figure C.17. Maximum Principal Strain at Time of Maximum Response - 19 foot Drop.

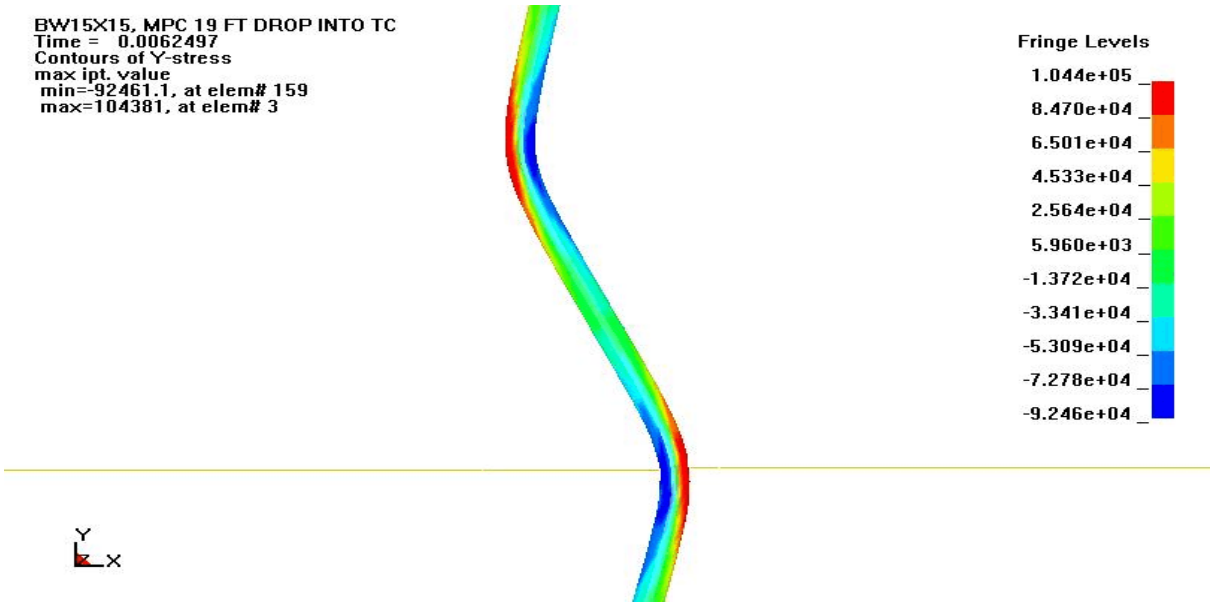

Figure C.18. Longitudinal Stress Distribution at Time of Maximum Response - 19 foot Drop.

C.1.4 Fuel Rod Cladding Failure

The cladding strain at failure (rupture or breach) of high burnup fuel, which is fuel with a burnup greater than 45 GWd/MTU, is expected to range from 1.0% to 3.0%. For the purpose of the PRA, the lower value of 1.0% strain is selected as the strain limit.

Appendix D of the PRA shows that the particulate release fraction from a spent fuel rod is a function of three variables: (1) the fraction of the fuel rim layer that fractures, (2) the percentage of particulate entrained by gasses during release, and (3) the number of tears (breaches) per rod. In addition, the fraction of the rim layer fractured and the number of breaches per rod are, in turn, functions of the g loads experienced by the fuel and the severity of the buckling that takes place during a given drop.

In a full-blown PRA each of these variables would be associated with a probability distribution and sampled as part of an overall simulation. However, because of the level of effort inherent in such an approach, Appendix D simplifies the methodology by recommending an upper bound value for release fractions to be used in the consequence analysis. This, in turn, simplifies the effort here in Appendix C by not requiring an estimate of the number of breaches per rod, but only whether or not the rod breaches at all. Also, since the analysis of fuel rod failure is based on a single pin model, it will be assumed that when one rod fails, all rods fail, although this is very unlikely.

For each drop height, Table C.3 lists the maximum principal strain in the cladding, the failure strain limit and whether or not fuel cladding breach occurs based on that limit strain.

Table C.3: Likelihood of Fuel Cladding Breach for Various Drop Scenarios .

Event Scenario	Impact Surface (Target)	Drop Height (feet)	Maximum Principal Strain in Cladding (in/in)	Strain Limit Selected for High Burnup Fuel	Fuel Cladding Breach
Transfer Cask Vertical Drop	Concrete Floor	1	0.0043	0.010	No
		5	0.0062	0.010	No
		20	0.0072	0.010	No
		40	0.011	0.010	Yes
		55	0.025	0.010	Yes
		70	0.037	0.010	Yes
		100	0.052	0.010	Yes
	Storage Overpack	5	(1)	na	No
		40	(1)	na	Yes
		80	(1)	na	Yes
MPC Drop into Storage Overpack	Storage Overpack Pedestal	19	0.090	0.010	Yes

(1): This drop was not evaluated for cladding response. Results for the transfer cask drop onto the concrete floor from the same height were used to determine cladding breach.

C.2 Fuel Response to Thermal Loads

The thermal analyses described in Section 4.2.3 of this report calculated the temperature of the fuel cladding for both the external fire and blocked vent scenarios. For these accident scenarios, fuel response is determined by comparing the calculated cladding temperatures to the temperature limits as discussed in Section 4.2.3. The long term normal and short term accident temperature limits for Zircalloy cladding are 400°C (752°F) and 570°C (1058°F), respectively.

In the case of an external fire, the short term temperature limit is used because the fire duration is only 3 hours. In the vent blockage scenario, the normal long term temperature limit is used because vent blockage is assumed to occur for 20 years for the purpose of the PRA only.

C.2.1 Results of Fuel Response to Thermal Loads

The thermal analyses performed for this PRA show that under normal steady state conditions the bulk MPC pressure is 0.565 MPa (82 psi) and the average fuel temperature is only 179°C (354°F). If the storage cask is exposed to an external fire for 3 hours the pressure increases slightly to 0.634 MPa (92 psi). Figures C.19 and C.20 plot the distribution of maximum cladding temperatures following a 3 hour fire. Figure C.19 shows the maximum cladding temperature as a function of axial height while Figure C.20 shows the maximum cladding temperature as a function of radial position from the cask center. The axial height is measured from the base of the overpack such that the bottom of the fuel rods is at a height of 0.67 m (2.2 ft). Also shown in these figures is the 570°C (1058°F) short term temperature limit. These figures clearly show that the cladding temperature limit is not exceeded. Therefore, no fuel failures occur if the storage cask is exposed to an external fire for 3 hours. (Note that cladding failure would not be expected to occur until cladding temperatures reached 750º C.)

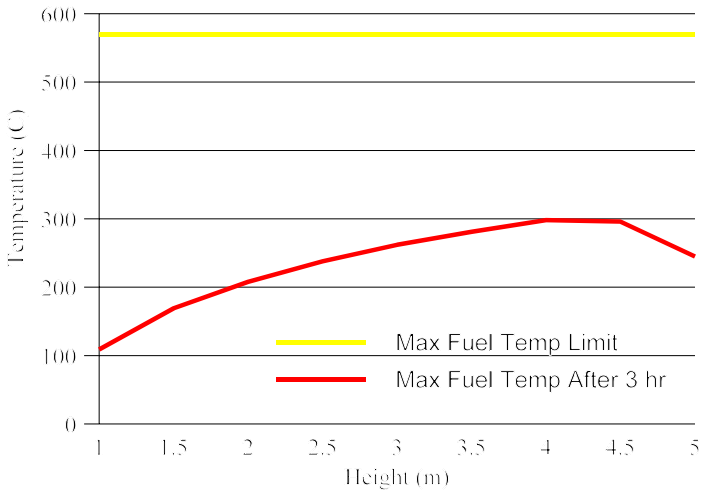

Figure C.19. Maximum Fuel Temperature as a Function of Axial Height after a 3 Hour External Fire

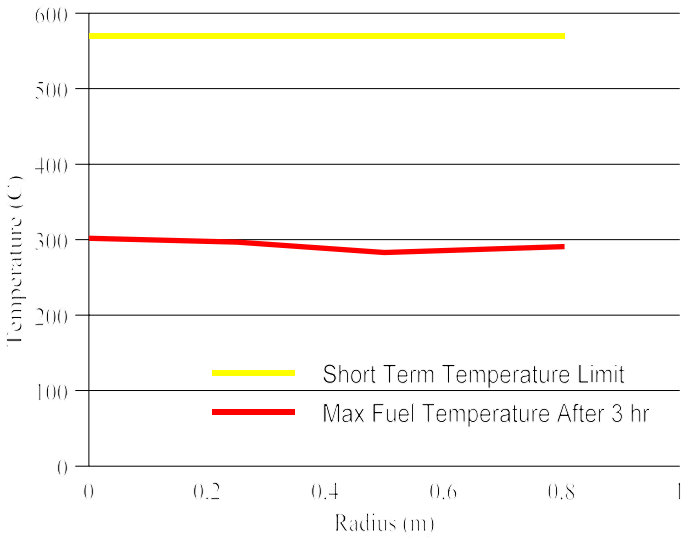

Figure C.20. Maximum Fuel Temperature as a Function of Radius after a 3 Hour External Fire

For the vent blockage scenario, the MPC pressure and cladding temperature are also expected to increase. For the purpose of this PRA, the assumption is made that vent blockage occurs for the entire 20 year license period of the cask. Under these conditions, the MPC pressure will eventually reach a new steady state value of 0.745 MPa (108 psi). Figure C.21 shows the maximum cladding temperature as a function of axial height after steady state vent blockage. Again the axial height is measured from the base of the overpack such that the bottom of the fuel rods is at a height of 0.67 m (2.2 ft). Figure C.22 plots the maximum cladding temperature as a function of radial position after vent blockage. These figures also show that none of the fuel within the cask will exceed the accident short temperature limit of 570°C (1058°F) for the vent

blockage scenario. The dashed line in Figure C.22 represents a polynomial fit (trend line) to the radial temperature distribution data. The equation of this polynomial fit is given below:

$$T_{Fuel} = -294.53 \bullet x^2 + 68.731 \bullet x + 462.01 \qquad [C.2]$$

where: T_{fuel} = Maximum fuel cladding temperature in °C
x = Radial distance from cask center in meters

The fit to the data is excellent with an R^2 value of 0.994.

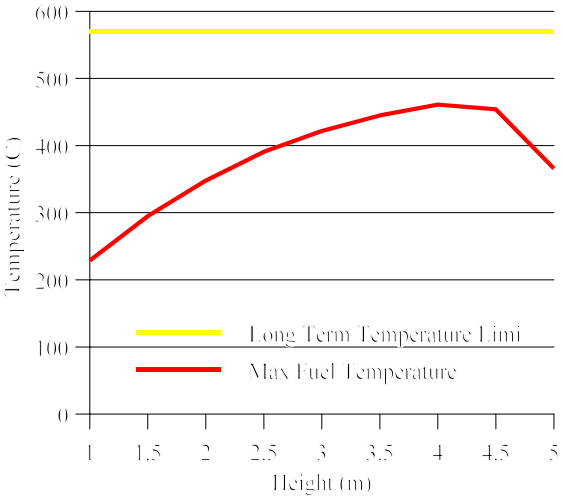

Figure C.21: Maximum Fuel Temperature with Vent Blockage as a Function of Axial Height.

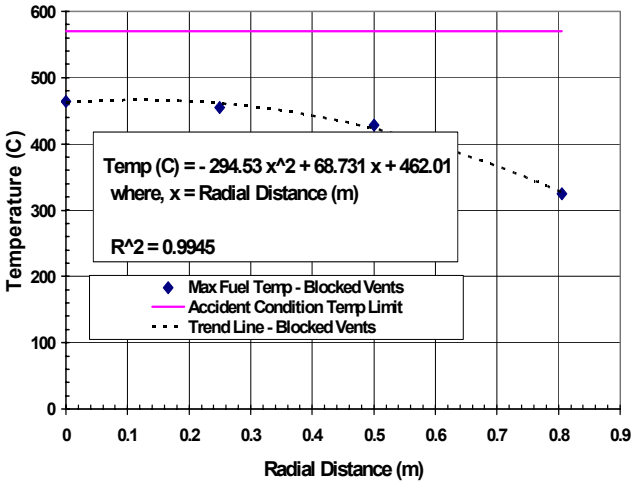

Figure C.22: Maximum Fuel Temperature as a Function of Radial Distance after Vent Blockage and Zircalloy Temperature Limit for Accident Condition.

References

1. Bjorkman, "The Buckling of Fuel Rods under Hypothetical Accident Conditions," Proceedings of PATRAM 2004, Berlin, Germany, September 2004.

2. HOLTEC Report HI-951312, HI-STORM Topical Safety Analysis Report, Revision 8.

3. Adkins, H.E., Koeppel,B.J., Tang, D.T., "Spent Nuclear Fuel Structural Response When Subject to an End Drop Impact Accident," Proceedings ASME/JSME Pressure Vessels and Piping Conference, PVP-Vol. 483, ASME, 2004.

4. KJ Geelhood and CE Beyer, Mechanical Properties of Irradiated Zircalloy, Transactions of ANS Winter Meeting, Vol 93, Washington, DC, Nov 2005

5. Sanders TL, KD Seager, YR Rashid, PR Barrett, AP Malinauskas, RE Einziger, H Jordan, TA Duffey, SH Sutherland, and PC Reardon. 1992. A Method for Determining the Spent-Fuel

Contribution to Transport Cask Containment Requirements. SAND90-2460, Sandia National Laboratories, Albuquerque, New Mexico.

6. US Nuclear Regulatory Commission (USNRC). 1999. Buckling of Irradiated Fuel Under Bottom End Drop Conditions. ISG 12, Rev 1, Washington, DC.

7. US Nuclear Regulatory Commission (USNRC). 2006. Buckling of Irradiated Fuel Under Bottom End Drop Conditions. ISG 12, Rev 2 (DRAFT), Washington, DC.

8. Electric Power Research Institute (EPRI). 1991. Fuel-Assembly Behavior Under Dynamic Impact Loads Due to Dry-Storage Cask Mishandling. EPRI-NP-7419, prepared by ABB Combustion Engineering, Inc. for Electric Power Research Institute, Palo Alto, CA.

9. Roark RJ, 1965. Formulas for Stress and Strain. 4th ed. McGraw-Hill, New York, NY

10. Jones, N., Structural Impact, Cambridge University Press, 1989.